*Supporting Information for*

# Porous Pt-M (M= Cu, Zn, Ni) nanoparticles as robust nanocatalysts†

Si-Bo Wang‡, Wei Zhu‡, Jun Ke, Jun Gu, An-Xiang Yin, Ya-Wen Zhang* and Chun-Hua Yan*

Beijing National Laboratory for Molecular Sciences, State Key Laboratory of Rare Earth Materials Chemistry and Applications, PKU-HKU Joint Laboratory in Rare Earth Materials and Bioinorganic Chemistry, College of Chemistry and Molecular Engineering, Peking University, Beijing 100871 China

## Experimental Section

### Synthesis

**Chemicals.** Oleylamine (OAm, >80%; Acros), potassium tetrachloroplatinate ($K_2PtCl_4$, A.R.; Shenyang Research Institute of Nonferrous Metal, China), methylamine ethanol solution (C.P.; Sinopharm Chemical Reagent Co. Ltd, China), ethanol (A.R.; Beijing Chemical Works, China), cyclohexane (A.R.; Beijing Chemical Works, China), hydrochloric acid (HCl, A.R.; Beijing Chemical Works, China), platinum(II) acetylacetonate ($Pt(acac)_2$, A.R.; Aldrich), cupric acetate monohydrate ($Cu(Ac)_2 \cdot H_2O$, A.R.; Beijing Chemical Works, China), cupric chloride dihydrate ($CuCl_2 \cdot 2H_2O$, A.R.; Sinopharm Chemical Reagent Co. Ltd, China), zinc chloride dihydrate ($ZnCl_2 \cdot 2H_2O$, A.R.; Shantou Xilong Chemical Factory, China), nickel(II) acetate tetrahydrate ($Ni(Ac)_2 \cdot 4H_2O$, A.R.; Beijing Chemical Works, China), titanium(IV) oxide (catalyst support, Alfa Aesar). The water used in the synthesis was ultrapure (Millipore, 18.2 MΩ).

**Synthesis of methyl substituted magnus' green salt (MSMGS, $[Pt(CH_3NH_2)_4][PtCl_4]$).** A few modifications were done to reported synthetic method (Ref. S1). 250 mg $K_2PtCl_4$ was dispersed in 10 mL of water in a flask. Then $K_2PtCl_4$ solution was heated to 60 ℃, and 4 mL of $CH_3NH_2$ ethanol solution (containing 27%-32% $CH_3NH_2$) was added. The jacinth solution turned to light yellow in a few minutes. The solution was heated to reflux at 90 ℃ for 1 h. After the solution cooled down (if certain precipitate appeared in the solution, a filtration procedure was needed), another 170 mg of $K_2PtCl_4$ was dissolved in 10 mL of water and was added into the colorless solution. A green precipitate was formed immediately as solutions were mixed. The precipitate was separated by vacuum filtration and washed by water and ethanol for several times. Then the green precipitate was recrystallized in 50 mL of 0.1 mol $L^{-1}$ HCl solution. During the recrystallization process, the solution turned orange as precipitate was completely dissolved. Green needle-like crystals were formed, when the solution cooled down naturally. The green crystal was separated with vacuum filtration and washed by water and ethanol. After that, the product was dried at 110 ℃ for 10 h. Elemental analysis results of C, H, and N (found (calcd) for $[Pt(CH_3NH_2)_4][PtCl_4]$: C, 7.39 (7.32); H, 3.14 (3.07); N, 8.50 (8.54).

**Synthesis of $[Pt(ethylenediamine)_2][PtCl_4]$.** The synthesis of $[Pt(ethylenediamine)_2][PtCl_4]$ was similar to that of MSMGS, except that we substituted ethylenediamine for $CH_3NH_2$ ethanol solution and the product is violet. Elemental analysis results of C, H, and N (found (calcd) for $[Pt(ethylenediamine)_2][PtCl_4]$): C, 7.56 (7.37); H, 2.39 (2.47); N, 8.59 (8.59).

**Synthesis of hollow Pt-Cu Nanoparticles (NPs).** OAm used in all reactions was previously purified in vacuum at 120 °C for 30 min. MSMGS (5 mg, 16.7 μmol, powder), $Cu(Ac)_2 \cdot H_2O$ (3.3 mg, 16.7 μmol, powder) and purified OAm (8.1 g, 10 mL) were mixed in a glass colorimetric tube (10 mL) with a stopper. After being stirred, the tube was sealed with a stopper and kept at 140 ℃ for one week. The black precipitates were separated by centrifugation (7800 rpm, 10 min), thoroughly washed with ethanol (40 mL) for three times, and dried in vacuum. If there are some products adhered to the wall or bottom of the tube, the precipitates can be washed with several milliliters of cyclohexane.

**Synthesis of Pt-Zn NPs.** The synthesis of Pt-Zn NPs was similar to that of Pt-Cu NPs, except that the same mole of $ZnCl_2 \cdot 2H_2O$ (2.87 mg, 16.7 μmol, powder) was used instead of $Cu(Ac)_2 \cdot H_2O$.

**Synthesis of Pt-Ni NPs.** The synthesis of Pt-Ni NPs was similar to that of Pt-Cu NPs, except that $Ni(Ac)_2 \cdot 4H_2O$ (1 mg, 4.2 μmol, powder) was used instead of $Cu(Ac)_2 \cdot H_2O$.

## Instrumentation

**TEM.** Samples for transmission electron microscopy (TEM) observations were prepared by drying a drop of diluted colloid dispersion of Pt-M NPs in cyclohexane on copper grids coated by amorphous carbon. Particle sizes and shapes were examined by a TEM (JEM-2100, JEOL, Japan) operated at 200 kV.

**HRTEM, EDS, HAADF-STEM and HAADF-STEM-EDS line scan.** Samples for energy dispersive X-ray spectroscopy (EDS) analysis and high angle annular dark field scanning transmission electron microscopy (HAADF-STEM) line scans were prepared by drying a drop of diluted Pt-Cu NPs on nickel grids. Then samples were loaded onto a Beryllium specimen holder for the further characterizations in order to eliminate the copper signals from the specimen holder. Pt-Zn and Pt-Ni samples were prepared with copper girds. High resolution TEM (HRTEM), EDS analysis, HAADF-STEM and HAADF-STEM-EDS line scans were performed on a FEG-TEM (JEM-2100F, JEOL, Japan) operated at 200 kV.

**ICP-AES.** Inductively coupled plasma-atomic emission spectroscopy (ICP-AES) analysis was performed on a Profile Spec ICP-AES spectrometer (Leeman, USA).

**PXRD.** The powder X-ray diffraction (PXRD) patterns of Pt-M NPs were obtained on a Rigaku D/MAX-2000 diffractometer (Japan) with a slit of 1/2 ° at a 2θ scan rate of 4 °·min$^{-1}$ under Cu $K_\alpha$ radiation (λ=1.5406 Å). Pt-M NPs dispersions in cyclohexane were previously dropped on glass slides for the preparation of PXRD measurement.

**BET.** The BET surface area tests were performed on a Micromeritics ASAP 2020 Accelerated Surface Area and Porosimetry Analyzer (Micromeritics, USA). NPs were pretreated at 200 ℃ for 4 h in air, and then $N_2$ adsorption/desorption curves were obtained at 78.3 K.

**IR.** The Fourier Transform infrared (FTIR) spectra of untreated and annealed porous Pt-Cu NPs/$TiO_2$ were conducted in Vector22 infrared spectrometer (Bruke, USA). The samples were prepared by mixing the catalysts powder with KBr and made into slices.

**EA.** Elemental analysis (EA) of the as-prepared Pt(II) precursors was performed with vario EL Elemental Analyzer (Elementar Analysensysteme GmbH, Germany).

## Catalytic Measurements

**Preparation of the Nanocatalyst.** The as-washed Pt-Cu NPs, Pt NPs, Cu NPs and Pt-Cu physically mixed NPs whose ratio of Pt to Cu is the same with Pt-Cu NPs (2 mg, determined by ICP-AES) were mixed with commercial $TiO_2$ support (1 g), and sonicated for 4 h at room temperature, then dried in vacuum. After that, the catalyst was heated in a crucible in the furnace at 180 ℃ for 8 h in air to remove the capping ligands on the surfaces of the NPs (Ref. S2). Then the NPs/$TiO_2$ catalysts were mixed with 2.5 g quartz sand for further catalytic test.

**CO Oxidation Reactions.** The activated and diluted catalyst was placed in a quartz tube filled with quartz sand of the homemade fixed bed reactor, connected with an on-line gas chromatograph

(Agilent 7890A, Agilent Technologies, USA) with installing a carbon molecular sieve column (Carboxen 1000, Supelco, USA). A thermal conductivity detector (TCD) was used to analyze the outlet gas compositions. The feed composition in the reactor was 1% CO (20.0%), 20% $O_2$ (99.995%), balance He (99.999%) and the flow rate was kept constant at 20 SCCM.

**Preferential CO Oxidation (PROX) Reactions.** The procedure was similar to that of CO oxidation reaction, except that the feed composition in the reactor was 2% CO (1.0%), 2% $O_2$ (99.995%), 50% $H_2$ (99.999%), balance He (99.999%) and the flow rate was kept constant at 50 SCCM.

**Calculation of Activity and Selectivity of PROX Reactions (Ref. S3).**

*CO conversion*, considering no side-reactions, can be defined as

$$X_{CO} = \frac{n_{CO}^{in} - n_{CO}^{out}}{n_{CO}^{in}} \times 100\% = \frac{n_{CO_2}^{out}}{n_{CO}^{in}} \times 100\% \qquad (1)$$

*Selectivity* is defined as the ratio of the oxygen converted to $CO_2$ to the total oxygen consumed as

$$S = \frac{n_{CO_2}^{out}}{2\left(n_{O_2}^{in} - n_{O_2}^{out}\right)} \times 100\% \qquad (2)$$

## Supplementary Data

***Table S1.*** EDS and ICP-AES results (atomic ratio) of porous Pt-Cu, Pt-Zn, and Pt-Ni NPs.

| | EDS | ICP-AES |
|---|---|---|
| **Pt-Cu NPs** | 19:81 | 21:79 |
| **Pt-Zn NPs** | 91:9 | 87:13 |
| **Pt-Ni NPs** | 56:44 | 58:42 |

***Table S2.*** BET surface areas ($S_{BET}$) of the metal NPs and $TiO_2$ support.

| | $S_{BET}$ / $m^2$ $g^{-1}$ |
|---|---|
| **Pt-Cu NPs** | 260 |
| **Pt NPs** | 6.6 |
| **Cu NPs** | 4.7 |
| **$TiO_2$** | 146 |

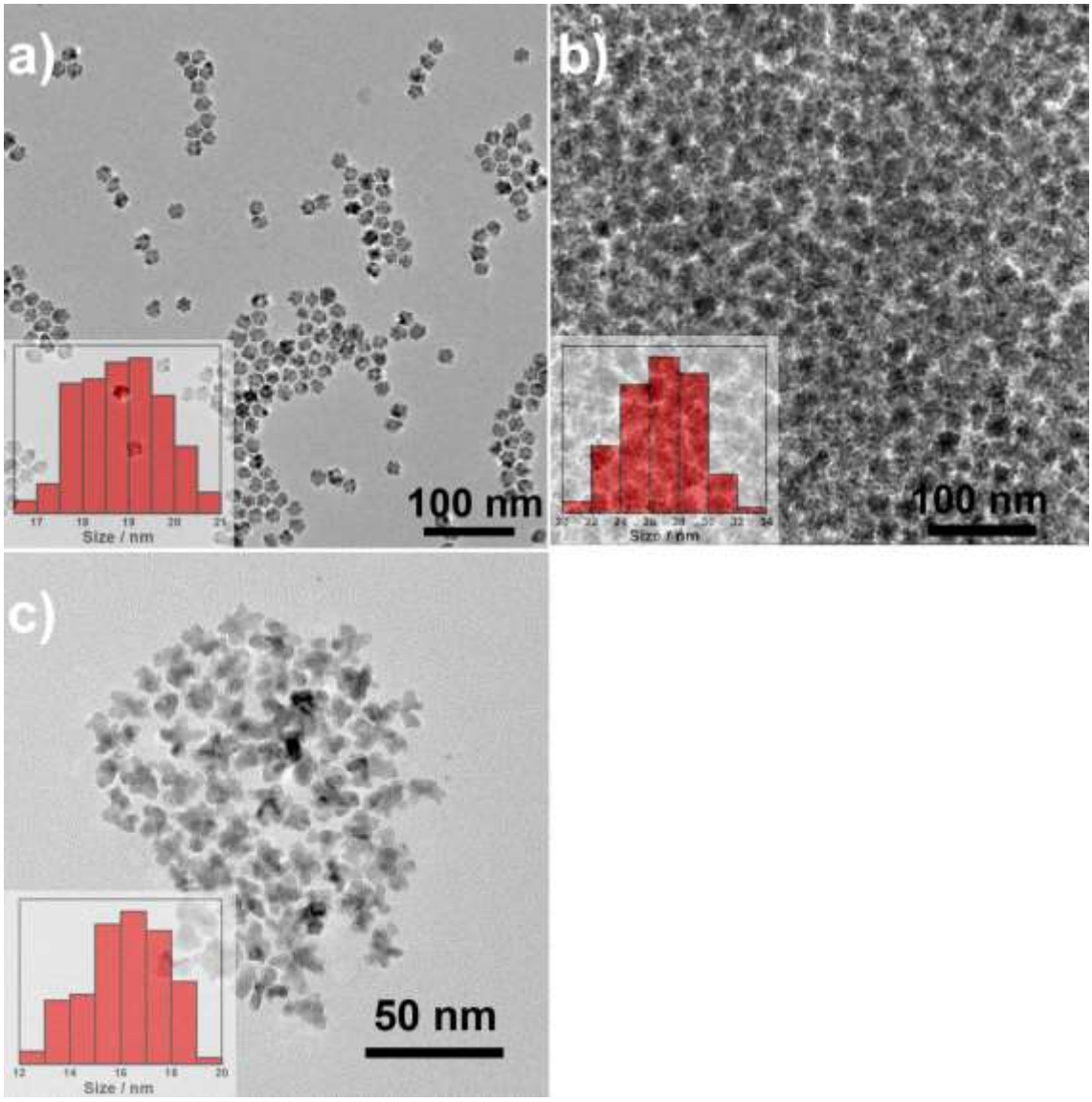


***Figure S1.*** Low-magnification TEM images of porous a) Pt-Cu, b) Pt-Zn, and c) Pt-Ni NPs (the insets are the size distributions of the NPs).

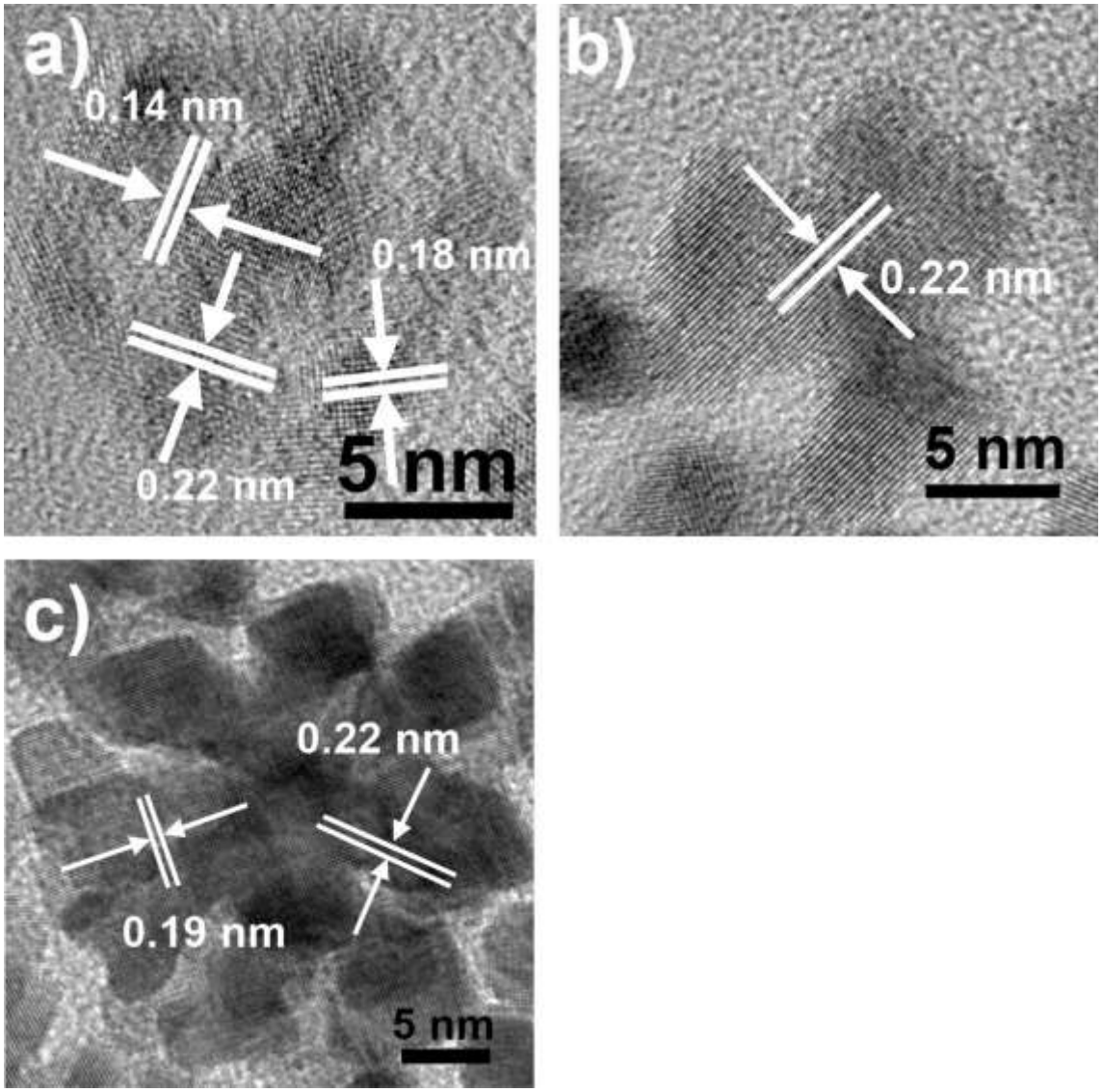


***Figure S2.*** HRTEM images of (a) Pt-Cu NPs, (b) Pt-Ni NPs and (c) Pt-Zn NPs. Compared with the interplanar spacing of Cu(111) plane (which is 0.21 nm), HRTEM image of porous Pt-Cu NPs shows obvious lattice expansion from the doping of Pt into Cu (0.22 nm for the (111) plane of $Pt_{0.2}Cu_{0.8}$ NPs). Doping with Zn or Ni into Pt, the lattice fringes of the (111) facets in Pt-Zn and Pt-Ni NPs were shorter than the interplanar spacing of Pt(111) plane (which is 0.23 nm).

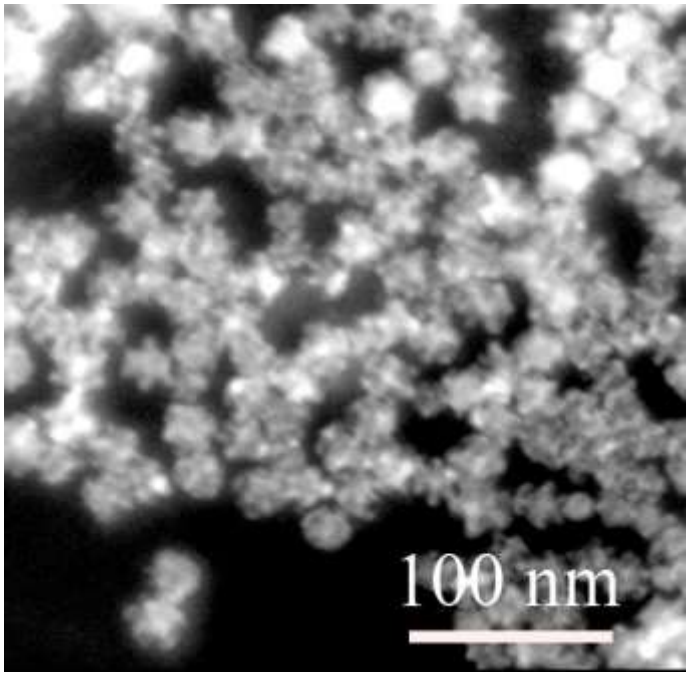


***Figure S3.*** HAADF-STEM image of Pt-Cu NPs.

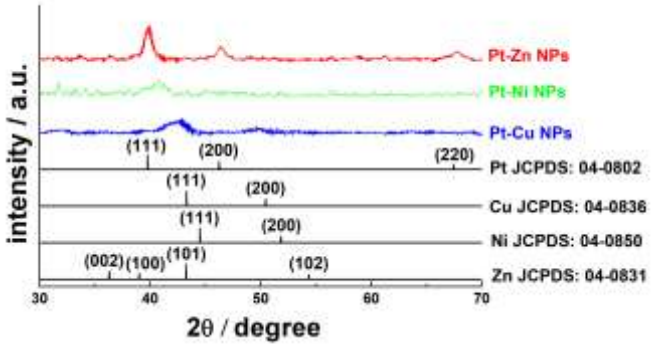


***Figure S4.*** PXRD patterns of Pt-M NPs with standard XRD data as references.

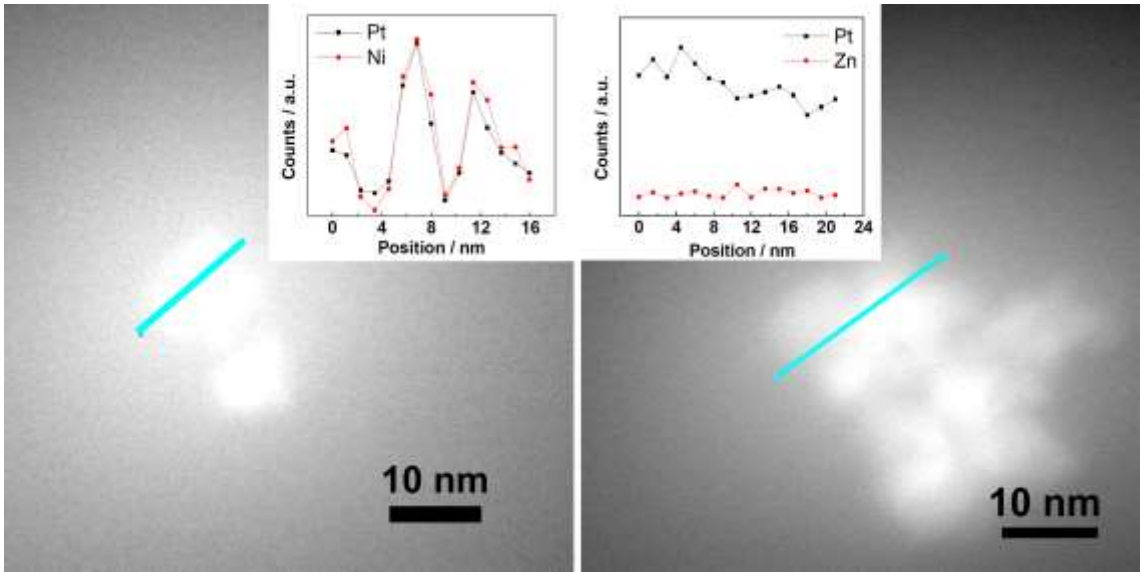


***Figure S5.*** HAADF-STEM-EDS line-scan profiles of (a) Pt-Ni and (b) Pt-Zn NPs.

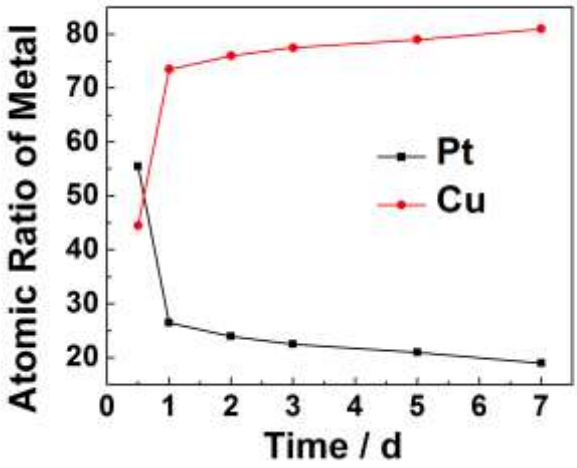


***Figure S6.*** Atomic ratios (ICP-AES results) of Pt and Cu in porous Pt-Cu NPs taken at different stages during synthesis.

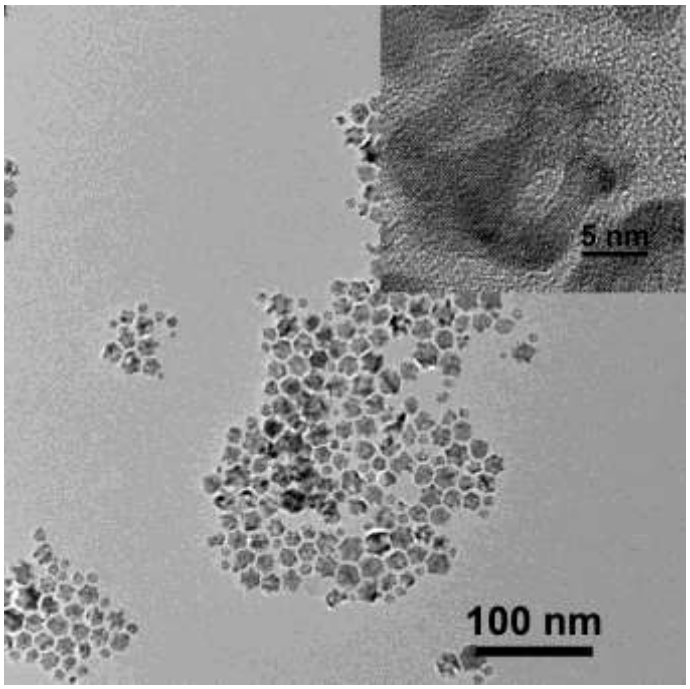


***Figure S7.*** TEM and HRTEM (inset) images of Pt-Cu NPs obtained under the reaction time of 14 days.

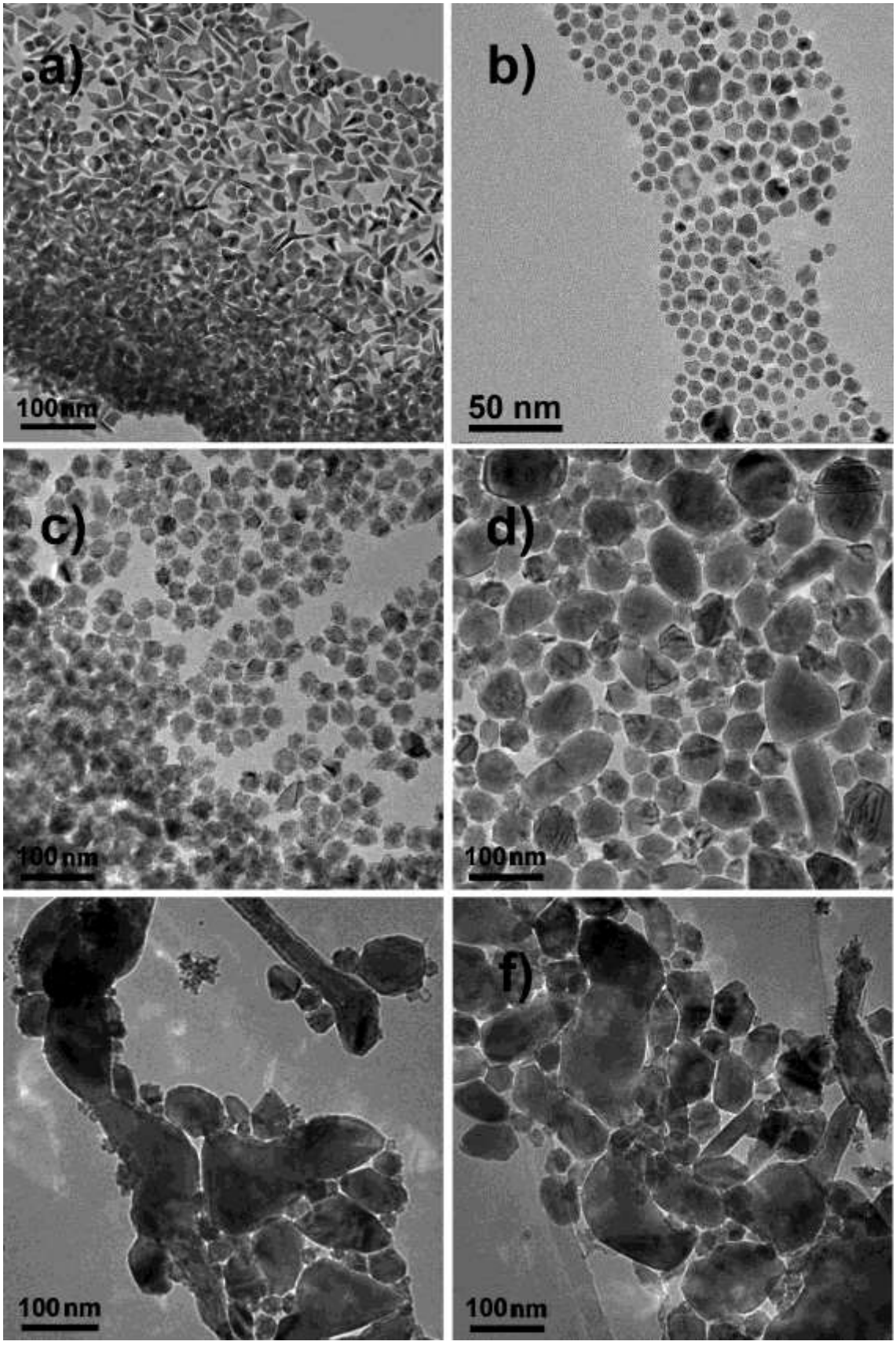


***Figure S8.*** TEM images of Pt-Cu NPs at different molar ratios of precursors: (a) without $Cu(Ac)_2$ $H_2O$; (b) Cu : Pt = 1 : 2; (c) Cu : Pt = 3 : 1; (d) Cu : Pt = 6 : 1; (e) Cu: Pt = 9: 1; (f) 3.33 mg $Cu(Ac)_2$ $H_2O$ without MSMGS. The absolute amounts of MSMGS were the same in all above synthesis except for the last one, and all the other conditions were the same.

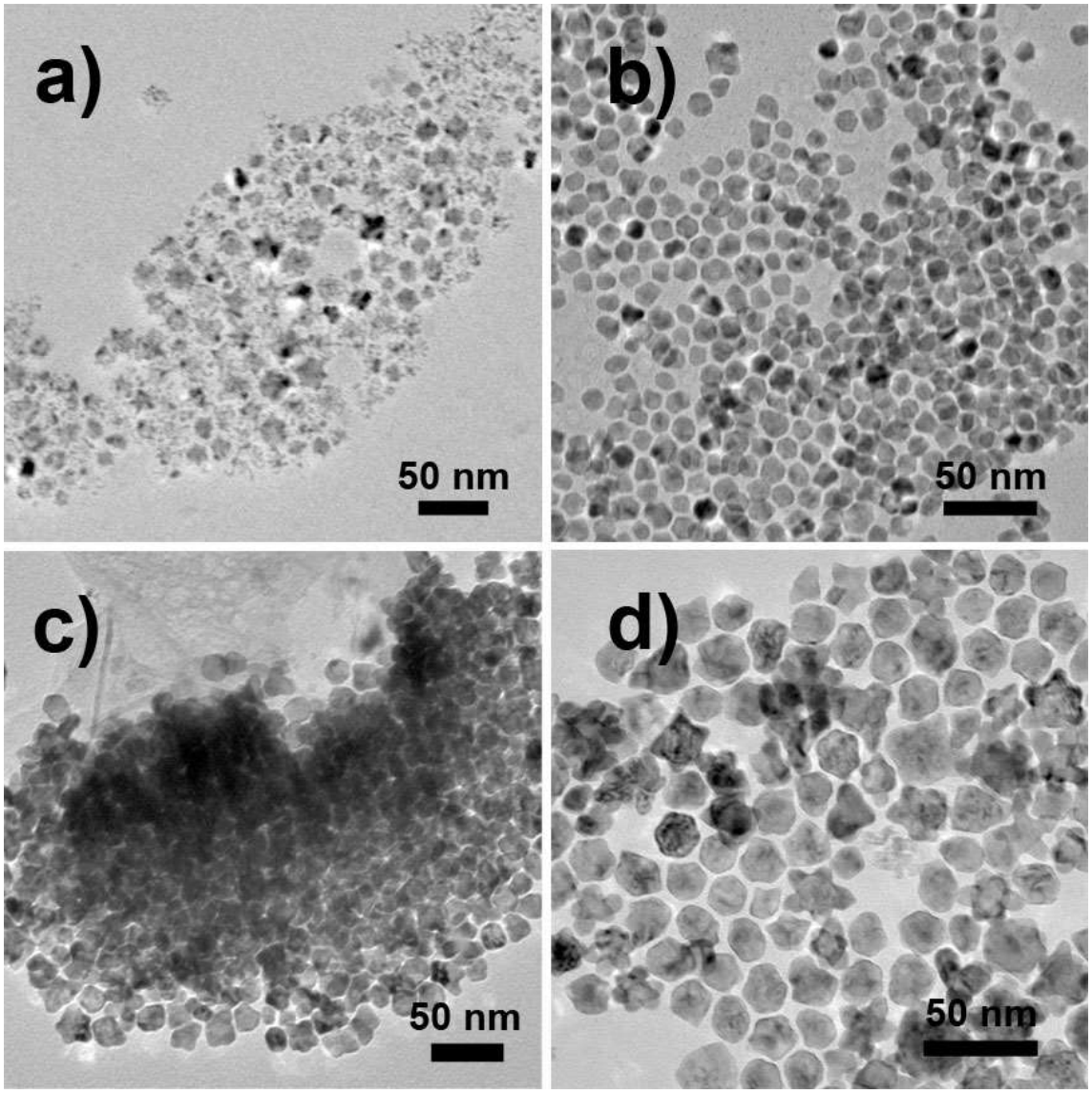


***Figure S9.*** TEM images of Pt-Cu NPs synthesized at different temperatures: (a) 130 ℃, (b) 150 ℃, (c) 160 ℃, (d) 170 ℃. All the other conditions were the same.

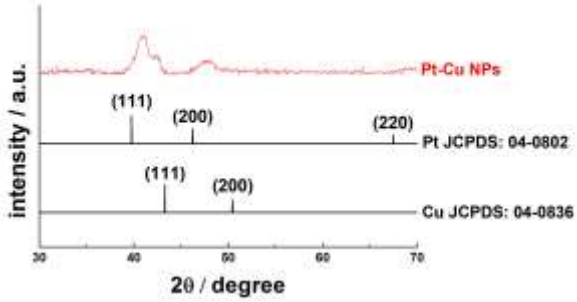


***Figure S10.*** PXRD pattern of Pt-Cu NPs synthesized at 170 ℃ with standard XRD data as references. It indicates that the Pt-Cu NPs synthesized at a higher temperature (>140℃) tended to be better crystallized, but occurred obvious phase segregation.

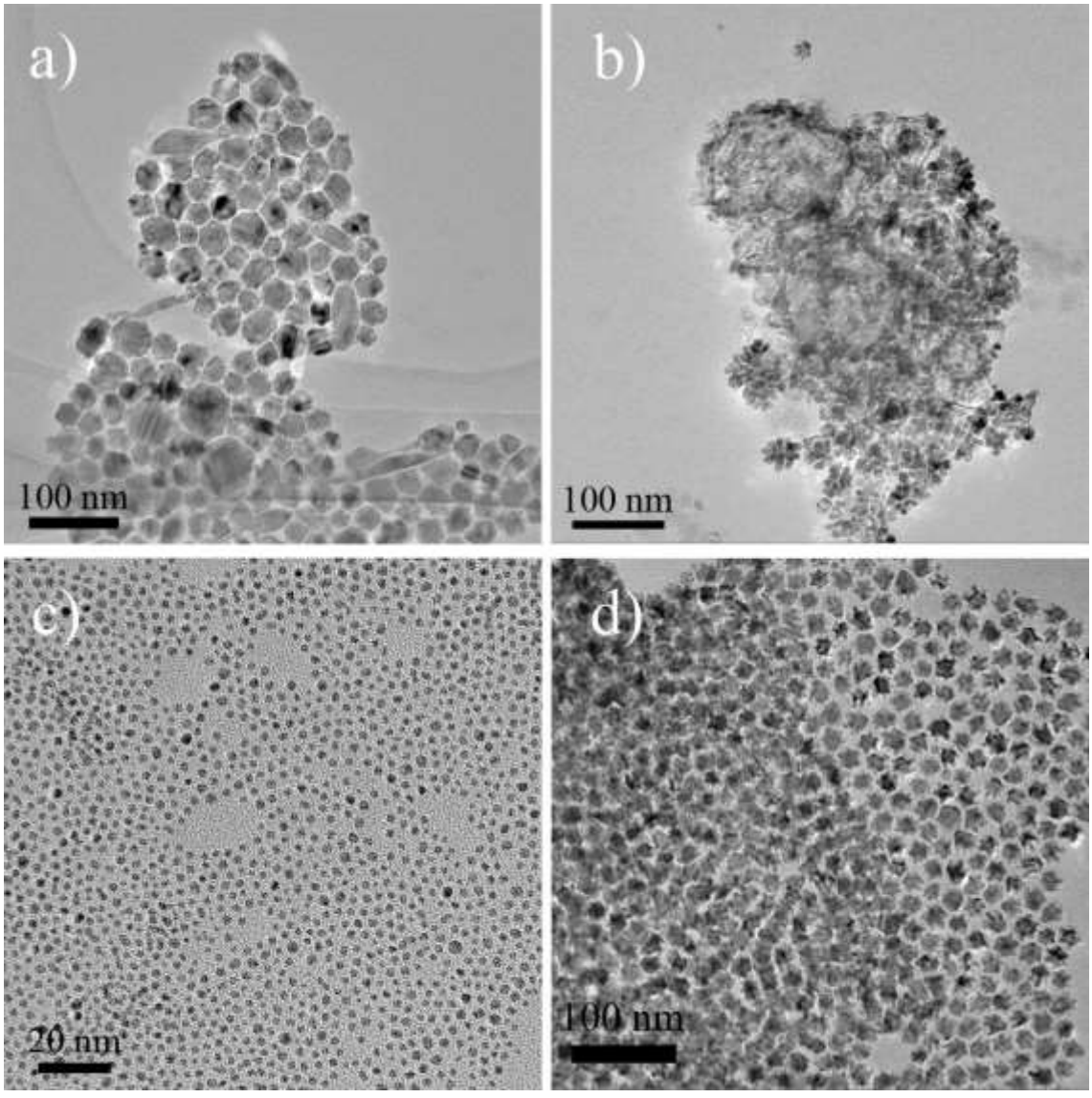


***Figure S11.*** TEM images of Pt-Cu NPs synthesized from different precursors: (a) with substituting [Pt(ethylenediamine)$_2$][PtCl$_4$] for MSMGS; (b) with substituting $K_2PtCl_4$ for MSMGS; (c) with substituting Pt(acac)$_2$ for MSMGS, (d) with substituting $CuCl_2$ for Cu(Ac)$_2$. All the other conditions were the same.

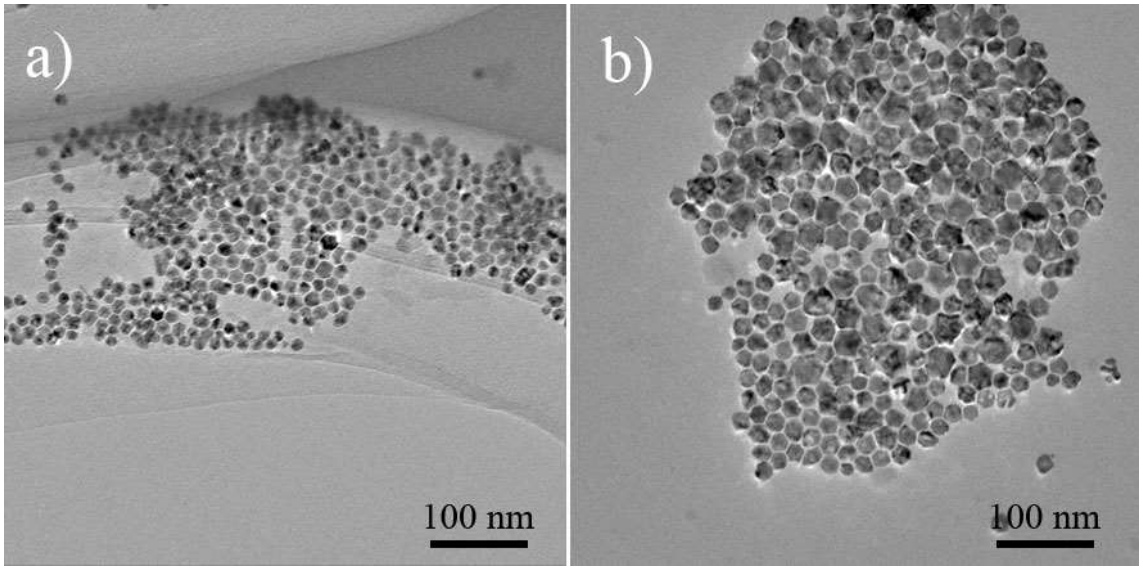


***Figure S12.*** TEM images of Pt-Cu NPs synthesized under different amounts of precursors: (a) using 8.3 μmol of each precursor; (b) using 33.3 μmol of each precursor. All the other conditions were the same.

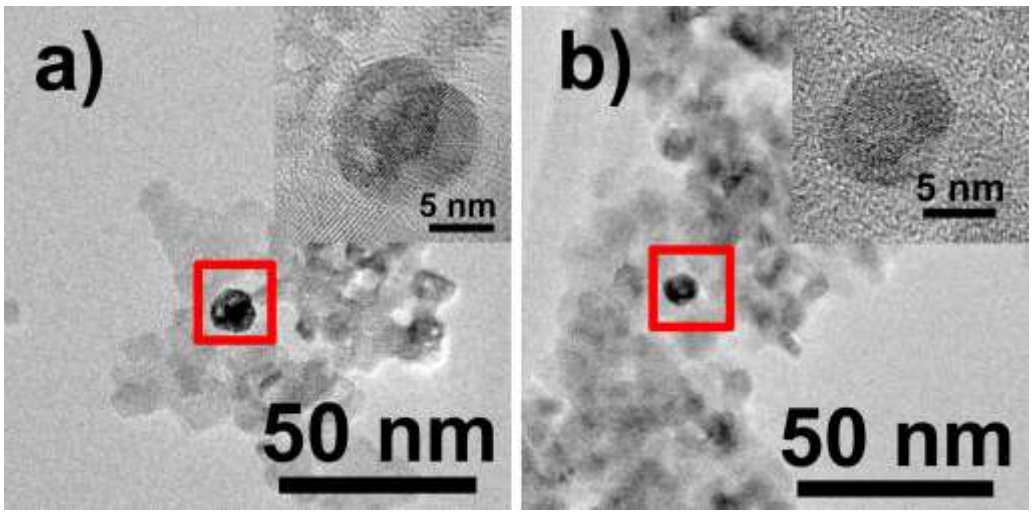


***Figure S13.*** TEM and HRTEM (insets) images of (a) untreated and (b) annealed Pt-Cu NPs/$TiO_2$. It indicates that, the porous Pt-Cu NPs maintained their morphology after loaded onto the $TiO_2$ support. However, the annealing treatment resulted in the partial collapse of pores and the decrease in the size of the NPs.

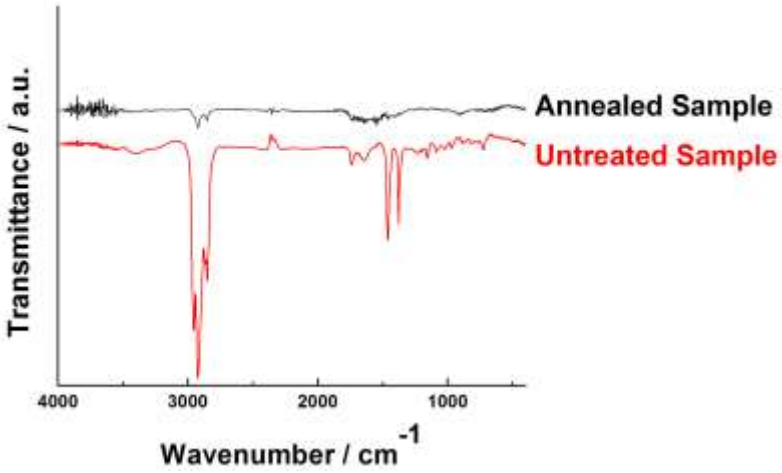


***Figure S14.*** FTIR spectra of annealed and untreated Pt-Cu NPs. It indicates that, after annealing treatment at 180 ℃ for 8 h, most of the OAm surfactant was removed for the surfaces of the porous Pt-Cu NPs as the catalyst.

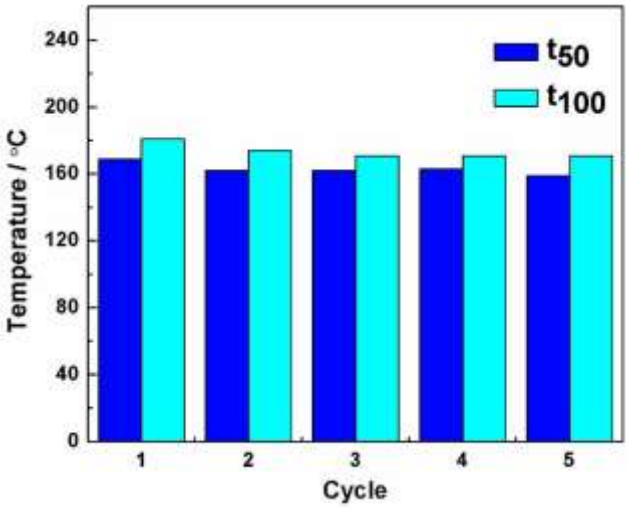


***Figure S15.*** Catalytic stability test of Pt-Cu NPs towards CO oxidation reaction.

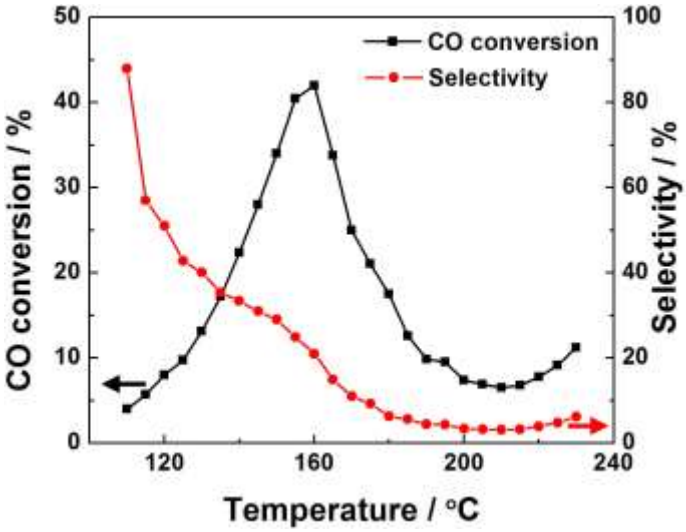


***Figure S16.*** CO conversion percentage and selectivity percentage of PROX reaction versus reaction temperature for the Pt-Cu NPs loaded onto commercial $TiO_2$ (0.2 wt %, both Pt and Cu included). The selectivity towards CO oxidation reaction decreases continuously as the temperature rises from 110 ℃ to 230 °C. Hence, a maximum selectivity of 90% is attained at a low temperature of 110 °C. It is also noted that the CO conversion percentages monotonically increases from 4% at 110 °C to 40% at 155 °C, and reaches a maximum of 42% at 160 °C. After 160 °C, the CO conversion percentages tend decreasing down to 3% as temperature increases. In addition, at the temperature higher than 220 °C, the CO conversion percentages increase once again due to the occurrence of the water gas shift reaction (WGSR) (Ref. S3).

**Ref. S1.** G. W. Watt, B. B. Hutchinson, D. S. Klett, *J. Am. Chem. Soc.*, **1967**, *89*, 9.
**Ref. S2.** D. G. Li, C. Wang, D. Tripkovic, S. H. Sun, N. M. Markovic, V. R. Stamenkovic, *ACS Catal.*, **2012**, *2*, 1358.
**Ref. S3**. F. Mariño, C. Descorme, D. Duprez, *Appl. Catal. B: Environ.*, **2004**, *54*, 59.